IBRO Reports 2 (2017) 63–71

Contents lists available at ScienceDirect

IBRO Reports

journal homepage: http://www.journals.elsevier.com/ibro-reports

Calmodulin modulates the Ca^{2+}-dependent inactivation and expression level of bovine $Ca_V2.2$ expressed in HEK293T cells

Chih-Hung Chi [a], Chih-Yung Tang [b,c], Chien-Yuan Pan [a,c,*]

[a] Department of Life Science, National Taiwan University, Taipei, Taiwan
[b] Department of Physiology, College of Medicine, National Taiwan University, Taipei, Taiwan
[c] Graduate Institute of Brain and Mind Sciences, National Taiwan University, Taipei, Taiwan

ARTICLE INFO

Article history:
Received 2 November 2016
Received in revised form 27 February 2017
Accepted 10 March 2017

Keywords:
Biotinylation
Ca^{2+}-dependent inactivation
Calmodulin
$Ca_V2.2$
Voltage-gated Ca^{2+} channels

ABSTRACT

Ca^{2+} influx through voltage-gated Ca^{2+} channels (Ca_Vs) at the plasma membrane is the major pathway responsible for the elevation of the intracellular Ca^{2+} concentration ($[Ca^{2+}]_i$), which activates various physiological activities. Calmodulin (CaM) is known to be involved in the Ca^{2+}-dependent inactivation (CDI) of several types of Ca_Vs; however, little is known about how CaM modulates $Ca_V2.2$. Here, we expressed $Ca_V2.2$ with CaM or CaM mutants with a Ca^{2+}-binding deficiency in HEK293T cells and measured the currents to characterize the CDI. The results showed that $Ca_V2.2$ displayed a fast inactivation with Ca^{2+} but not Ba^{2+} as the charge carrier; when $Ca_V2.2$ was co-expressed with CaM mutants with a Ca^{2+}-binding deficiency, the level of inactivation decreased. Using glutathione S-transferase-tagged CaM or CaM mutants as the bait, we found that CaM could interact with the intracellular C-terminal fragment of $Ca_V2.2$ in the presence or absence of Ca^{2+}. However, CaM and its mutants could not interact with this fragment when mutations were generated in the conserved amino acid residues of the CaM-binding site. $Ca_V2.2$ with mutations in the CaM-binding site showed a greatly reduced current that could be rescued by CaM_{12} (Ca^{2+}-binding deficiency at the N-lobe) overexpression; in addition, CaM_{12} enhanced the total expression level of $Ca_V2.2$, but the ratio of $Ca_V2.2$ present in the membrane to the total fraction remained unchanged. Together, our data suggest that CaM, with different Ca^{2+}-binding abilities, modulates not only the inactivation of $Ca_V2.2$ but also its expression to regulate Ca^{2+}-related physiological activities.

© 2017 The Authors. Published by Elsevier Ltd on behalf of International Brain Research Organization. This is an open access article under the CC BY-NC-ND license (http://creativecommons.org/licenses/by-nc-nd/4.0/).

1. Introduction

Intracellular Ca^{2+} concentration ($[Ca^{2+}]_i$) changes are an important signal for a wide spectrum of cell activities from short-term neurotransmitter release to long-term control of gene expression (Berridge, 2014; Lian and Zheng, 2016; Mintz et al., 1995; Simms and Zamponi, 2014; Soderling and Derkach, 2000; Yagami et al., 2012). The voltage-gated Ca^{2+} channels (Ca_Vs) at the plasma membrane are encoded by various isoforms in different cells and are the main pathway for Ca^{2+} influx. One of the Ca_V isoforms, Ca_V2, is widely expressed in the central and peripheral nervous system (Coppola et al., 1994; Fujita et al., 1993; Mills et al., 1994; Westenbroek et al., 1992, 1998) and is involved in synaptic transmission in most neurons (Dunlap et al., 1995; Olivera et al., 1994).

The opening of the Ca_Vs elevates the $[Ca^{2+}]_i$ to a μM level upon membrane depolarization from a resting level of approximately 50 nM (Simons, 1988). Both the Ca_V1s and Ca_V2s show Ca^{2+}-dependent inactivation (CDI), and calmodulin (CaM), which has 4 EF-hand Ca^{2+} binding motifs, may play a role in this inactivation (Johny et al., 2013; Peterson et al., 1999; Soong et al., 2002; Tadross et al., 2008). CaM binds to the IQ motifs located at the C-terminals of several subtypes of voltage-gated Na^+ and Ca^{2+} channels to regulate the channel activity in a Ca^{2+}-dependent manner (Ben-Johny et al., 2015). CDI is a typical feedback inhibition for Ca^{2+} homeostasis (Eckert and Chad, 1984; Eckert and Tillotson, 1981; Tillotson, 1979; Zweifach and Lewis, 1995); in contrast, Ca^{2+} signaling also induces facilitation (Ca^{2+}-dependent facilitation, CDF) in several types of Ca_Vs (Chaudhuri et al., 2007; Lee et al., 2000).

$Ca_V2.2$ shows CDI and voltage-dependent inactivation (VDI), but no CDF has been reported (Ben-Johny and Yue, 2014). Similar to other Ca_Vs, the CDI is mediated by CaM, but the detailed interaction is not clear. In this report, we verified that bovine $Ca_V2.2$ showed an apparent CDI, and CaM interacted with the intracellular C-terminal of $Ca_V2.2$ ($Ca_V2.2$-CT). Mutating the IF residues in the IQ motif to

* Corresponding author. Department of Life Science, National Taiwan University, 1 Sec. 4, Roosevelt Road, Taipei, 10617, Taiwan.
E-mail address: cypan@ntu.edu.tw (C.-H. Chi).

http://dx.doi.org/10.1016/j.ibror.2017.03.002
2451-8301/© 2017 The Authors. Published by Elsevier Ltd on behalf of International Brain Research Organization. This is an open access article under the CC BY-NC-ND license (http://creativecommons.org/licenses/by-nc-nd/4.0/).

AF ($Ca_V2.2^{IF/AF}$) or AA ($Ca_V2.2^{IF/AA}$) not only decreased the current amplitude but also abolished the interaction with CaM. However, the co-expression of CaM_{12} (Ca^{2+}-binding deficiency at the N-lobe), which has a Ca^{2+}-binding deficiency in the N-lobe, enhanced the currents of $Ca_V2.2$ and its mutants. Thus, these results reveal that the C- and N-terminals of CaM have differential effects on binding to $Ca_V2.2$ and regulating the channel activities.

2. Material and methods

2.1. Chemicals

Lipofectamine 2000, mouse monoclonal antibodies against the CaM and glutathione S-transferase (GST), Dulbecco's modified Eagle's medium, and other chemicals for cell culture were obtained from Invitrogen Inc. (Carlsbad, CA, USA). Mouse monoclonal antibodies against the Flag epitope and all additional chemicals, unless otherwise indicated, were purchased from Sigma-Aldrich Inc. (St. Louis, MO, USA).

2.2. Plasmid preparation

The plasmids for bovine $Ca_V2.2$ and their accessory subunits were generously provided by Dr. Aaron P. Fox (University of Chicago) (Currie and Fox, 2002). The protocol used to prepare rat brain cDNA and mutants of CaM was described previously using Pfu Ultra AD polymerase (Agilent Technologies, USA) (Lin et al., 2013; Shih et al., 2009). The primers for the AF mutant were (Forward) CGCAGCTCTGATGGCATTCGACTTCTACAA and (Reverse) TAGAAGTCGAATGCCATCAGAGCTGCGTACACC ; the primers for the AA mutant were (Forward) CTGATGGCAGCCGACTTCTACAAACAGAAC and (Reverse) GAAGTCGGCTGCCATCAGAGCTGCGTACACC (shaded nucleotides indicate the mutated IF sequence). The triple-Flag-tagged $Ca_V2.2$s (T-$Ca_V2.2$s) were constructed by digesting a synthetic dsDNA (TCTAGACTTAAGACCGGTGCCACCATG GATTACAAGGATGACGACGATAAGGACTATAAGGACGATGATGACAAGGAC/TACAAAGATGATGACGATAAAG AATTCAAGCTTACCGGTATGGTCCGCTTCGGGGACGAGCTGGGCGGCCGCGGATCC, gene synthesized by Thermo Fisher Scientific, the underline indicates the triple-Flag sequence) with *AflII* and *NotI* sites and inserting the fragment at the 5′-terminal of $Ca_V2.2$. The clones with the intracellular C-terminal segment of T-$Ca_V2.2$s were digested with *EcoRI* from T-$Ca_V2.2$s (aa 1710-2332, gene number: NM_174632.2).

The primers for cloning the *CaM* from the rat brain were (Forward) GGGATCCATGGCTGATCAGCTGACT (BamHI) and (Reverse) CTCTAGATCATTTTGCAGTCATCAT (XbaI) (shaded nucleotides indicated the restriction enzyme site); the construct was then subcloned into pcDNA3.1 plasmid. To synthesize the Ca^{2+}-binding deficiency mutation, we mutated the last a.a., glutamate, of each EF-hand motif to glutamine using the following primers: EF1 Forward ATCACAACAAAGCAGCTG and Reverse AGTCCCCAGCTGCTTTGT ; EF2 Forward ATTGACTTCCCACAGTTC and Reverse AGTCAAGAACTGTGGGAA ; EF3 Forward ATCAGTGCGGCACAACTG and Reverse GTGGCGCAGTTGTGCCGC ; EF4 Forward GTCAACTATGAACAATTC, and Reverse CTGTACGAATTGTTCATA (shaded nucleotides indicate the mutated ones). All of the primers listed are in the 5′ to 3′ direction.

2.3. Transfection of HEK293T cells

For transient expression of the genes in HEK293T cells grown in a 35-mm dish, we mixed α_{1B}, β_{2a}, and $\alpha_2\delta$ (1 μg total at a ratio of 1:1:1 and 0.1 μg of a green fluorescence protein (GFP) plasmid) with Lipofectamine 2000 according to the manufacturer's instructions. We used GFP fluorescence to identify transfected cells and performed experiments 24–36 h after transfection.

2.4. Protein extraction

HEK293T cells were dissolved in a lysis buffer (150 mM NaCl, 1% NP-40, 0.5% sodium deoxycholate, 0.1% SDS, and 50 mM Tris, pH 7.5, Bioman Inc., Taiwan) containing a protease inhibitor cocktail (Set V, 1:100 dilution, Calbiochem, La Jolla, California, USA). The lysates were centrifuged at 1000 ×*g* for 30 min, and the supernatant was collected as the total lysate.

2.5. GST pulldown assays

We purified the GST-fused CaM, CaM_{12}, CaM_{34} or CaM_{1234} (has no Ca^{2+}-binding ability at both the N- and C-lobes) expressed in *E. coli* as described previously (Chou et al., 2015) and used a Bradford-based protein assay kit (Bio-Rad, USA) to determine the protein concentration. To pull down interacting proteins, we incubated the GST-fused protein or GST with GSH-Sepharose 4B beads (GF Healthcare, USA) following the protocol suggested by the manufacturer. We mixed the beads with cell lysate at room temperature for 1 h or 4 °C overnight in a lysis buffer. The proteins that bound to the beads were analyzed by sodium dodecyl sulfate polyacrylamide gel electrophoresis (SDS-PAGE) followed by Western blotting.

2.6. Electrophysiological recording

The recording procedure was described previously (Shih et al., 2009). The recordings were performed at room temperature with an EPC-10 amplifier and were controlled by the Pulse program (HEKA Elektronik, Lambrecht/Pfalz, Germany). In brief, a cell was incubated in NMG buffer (in mM, 130 NMG, 20 glucose, 10 HEPES, 1 $MgCl_2{\cdot}6H_2O$, 2 KCl, 10 $CaCl_2{\cdot}2H_2O$, pH 7.2 with KOH, 300–305 mOsm) and patched in whole-cell mode. For the Ba^{2+} current measurement, Ca^{2+} was replaced with 10 mM Ba^{2+}. The membrane potential was held at −70 mV and depolarized to various potentials for channel activation. The pipette solution consisted of (in mM) 120 aspartic acid, 5 $MgCl_2$, 40 HEPES, 0.1 EGTA, 2 ATP, and 0.3 GTP, pH 7.3 with CsOH (310 mOsm/kg). The R_{250} ratio was measured by holding at −70 mV and depolarizing for 250 ms from −50 to +120 mV. The activation curves were created from the tail currents obtained by a 10-ms depolarization to various potentials and used for the analysis of $V_{1/2}$ and slope.

2.7. Biotinylation

The HEK293T cells were seeded on poly-L-lysine-coated 35-mm dishes and transfected with different plasmids as previously described. The cells were incubated on ice and washed with D-PBS buffer supplemented with 0.5 mM $CaCl_2$ and 2 mM $MgCl_2$, followed by 1 mg/mL sulfo-NHS-LC-biotin (Thermo Fisher Scientific) in 1 mL of D-PBS on ice with gentle rocking for 1 h. After being washed with 100 mM of glycine in PBS (in mM, 142 NaCl, 2 KCl, 8 $Na_2HPO_4{\cdot}7H_2O$, and 1.5 $NaH_2PO_4{\cdot}H_2O$, pH 7.2) two times and TBS (in mM, 20 Tris-HCl, and 150 NaCl, pH 7.4) one time, solubilization was performed using 400 μL of lysis buffer (in mM, 150 NaCl, 5 EDTA, and 50 Tris-HCl, pH 7.6 and 1% Triton-X 100 with dithiothreitol, 1 phenylmethylsulfonyl fluoride and protease inhibitors). The cell lysates were incubated with 30 μL streptavidin-agarose beads (Thermo Scientific) overnight at 4 °C. The beads were washed once in lysis buffer, followed by another wash in high salt buffer (in mM, 500 NaCl, 5 EDTA, and 50 Tris-HCl, pH 7.6 and 0.1% Triton-X 100) and low salt buffer (in mM, 2 EDTA, and 10 Tris-HCl, pH 7.6 and

0.1% Triton-X 100). Then, Laemmli sample buffer (containing 6% SDS) was added to the samples, and the samples were boiled at 70 °C for 10 min and prepared for Western blot analysis.

2.8. Statistical analysis

Data are presented as the mean ± SEM from at least three different batches of cells and were analyzed by one-way ANOVA with Fisher's post hoc test. Differences were considered significant when the p value was less than 0.05.

3. Results

3.1. Bovine $Ca_V2.2$ shows Ca^{2+}-dependent inactivation

To examine the inactivation of bovine $Ca_V2.2$ currents, we expressed bovine α_{1B} and accessory subunits in HEK293T cells and measured the whole-cell currents in buffers containing Ca^{2+} or Ba^{2+} as the charge carrier (Fig. 1). When depolarized to various potentials for 250 ms from a holding potential of −70 mV, the representative current traces of cells incubated in buffer containing Ca^{2+} but not Ba^{2+} showed a fast inactivation after reaching the maxima (Fig. 1A). The current-voltage relationship showed that the depolarization potential for the maximum peak inward current was +30 mV for $Ca_V2.2$ using either Ca^{2+} or Ba^{2+} as the charge carrier (Fig. 1B). The residual currents at the end of the depolarization (R_{250}) of a representative cell were 27.8 or 77.5% of the peak current using Ca^{2+} (R_{250}/Ca^{2+}) or Ba^{2+} (R_{250}/Ba^{2+}), respectively, as the charge carrier at a depolarization potential of +30 mV (Fig. 1C). Fig. 1D shows that the average R_{250}/Ca^{2+} and R_{250}/Ba^{2+} were 17.4 ± 2.3 (n = 31) and 79.0 ± 2.5% (n = 15), respectively. These results demonstrate that Ca^{2+} is responsible for the majority of the inactivation of bovine $Ca_V2.2$ currents.

3.2. Both lobes of CaM modulate the CDI effect

CaM has 4 Ca^{2+} binding sites with 2 at each of the N- or C-lobes, and each lobe has different effects in modulating various Ca_Vs (Ben-Johny et al., 2015; Yang et al., 2006). To verify the effect of each lobe of CaM in regulating $Ca_V2.2$, we measured the $Ca_V2.2$ currents using Ca^{2+} or Ba^{2+} as the charge carrier with co-expression of CaM or Ca^{2+}-binding-deficient mutants in HEK293T cells (Fig. 2 & Table 1). The

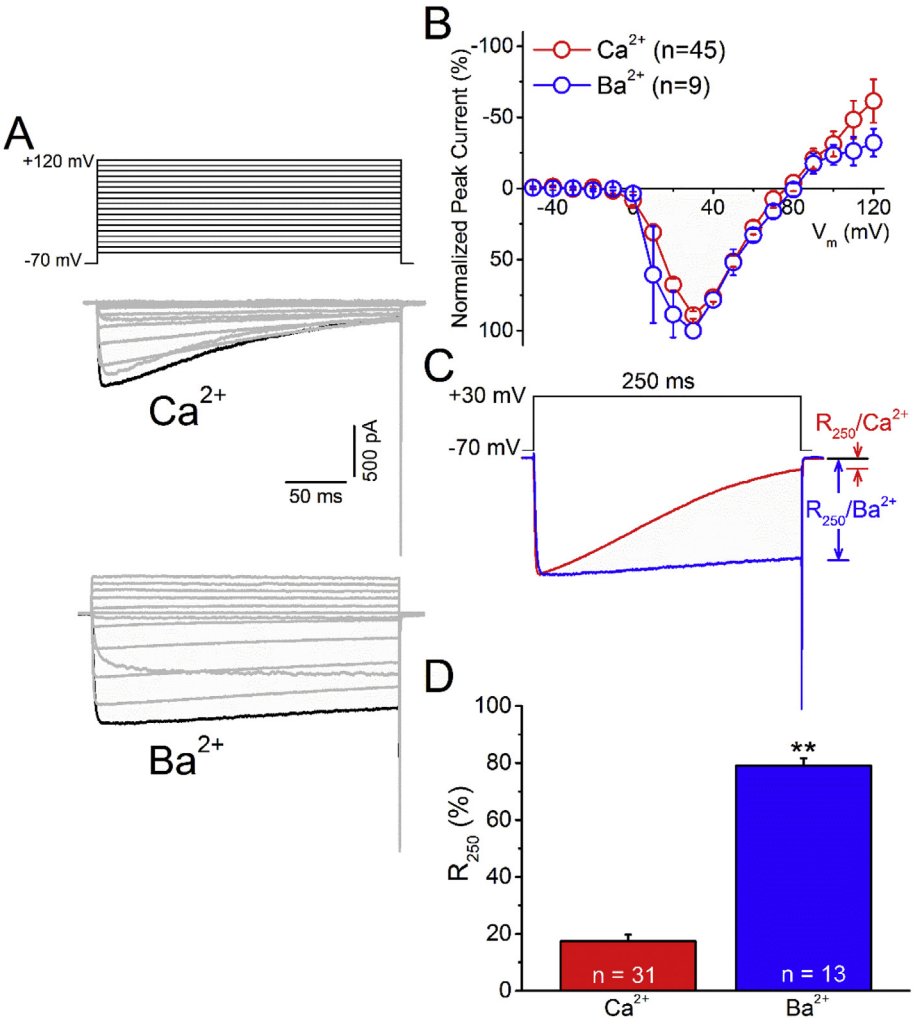

Fig. 1. Bovine $Ca_V2.2$ shows Ca^{2+}-dependent inactivation. HEK293T cells transfected with $Ca_V2.2$ were whole-cell patched in voltage-clamp mode and depolarized to various potentials from a holding potential of −70 mV for 250 ms. A. The current traces of a representative cell at different potentials using Ca^{2+} (middle panel) or Ba^{2+} (bottom panel) as the charge carrier. The black line indicates the trace obtained at +30 mV. B. The normalized current-voltage relationship. The peak inward current measured using Ca^{2+} (n = 45) or Ba^{2+} (n = 9) as the charge carrier at different potentials was normalized to the respective maxima of each single cell and then averaged. C. The current evoked by a step depolarization from −70 to +30 mV for 250 ms was recorded using Ca^{2+} (red) or Ba^{2+} (blue) as the charge carrier. The residual current at the end of the depolarization was normalized to the peak current as the R_{250}/Ca^{2+} or R_{250}/Ba^{2+}. D. The average R_{250}/Ca^{2+} and R_{250}/Ba^{2+} of $Ca_V2.2$. Data are presented as the mean ± SEM. **, $p < 0.01$ compared to the Ca^{2+} group using Student's t-test.

results indicated that the current traces in cells expressing CaM showed an apparent inactivation when using Ca^{2+} as the charge carrier; in contrast, the inactivation level was decreased in cells expressing CaM_{12}, CaM_{34}, and CaM_{1234} with Ca^{2+}-binding deficiencies at the N-lobe, C-lobe, and both, respectively. The results (Fig. 2D & Table 1) showed that CaM mutants, CaM_{12}, CaM_{34}, and CaM_{1234}, all showed a significant increase in R_{250}/Ca^{2+}. In contrast, CaM and CaM_{12} significantly lowered the R_{250}/Ba^{2+}; CaM_{34} and CaM_{1234} had no effect on the R_{250}/Ba^{2+}. However, CaM and CaM_{12} significantly decreased and increased, respectively, the peak inward current at +30 mV (I_{30}/Ca^{2+}) when using Ca^{2+} as the charge carrier; CaM_{34} and CaM_{1234} had no effect when compared with that of the $Ca_V2.2$ alone. However, using Ba^{2+} as the charge carrier enhanced the current density (I_{30}/Ba^{2+}) except in the co-expression of CaM_{12} (Table SI). These results suggest that the N- and C-lobes of CaM have differential effects in modulating the current amplitude and inactivation.

3.3. Mutating the IF residues reduces the current amplitude

The IQ motif of Ca_V1s and $Ca_V2.1$ is responsible for CaM binding and the CDI effect (Ben-Johny et al., 2015). To assess the importance of this motif of $Ca_V2.2$, we expressed $Ca_V2.2^{IF/AF}$ or $Ca_V2.2^{IF/AA}$ in HEK293T cells and measured the currents after depolarization to different potentials for 250 ms (Fig. 3 and Table 1). The normalized current-voltage relationship (Fig. 3B) showed that the voltages of the maximum inward current were positively shifted in these mutants. The activation curves (Fig. 3D and Table 1) showed that the $V_{1/2}$ values were significantly shifted from 18.7 ± 2.7 mV (n = 20) with wild-type $Ca_V2.2$ to 31.6 ± 1.9 mV (n = 7, $p < 0.01$) and 41.4 ± 2.0 mV (n = 6, $p < 0.01$) with $Ca_V2.2^{IF/AF}$ and $Ca_V2.2^{IF/AA}$, respectively. The I_{30}/Ca^{2+} of $Ca_V2.2^{IF/AF}$ and $Ca_V2.2^{IF/AA}$ was significantly reduced to −38.5 ± 9.4 pA/pF (n = 17, $p < 0.05$) and −13.4 ± 3.3 pA/pF (n = 9, $p < 0.001$), respectively, from that of the wild-type, with a value of −71.1 ± 8.4 pA/pF (n = 37). Therefore, the conserved IF residues are important in maintaining the current amplitude and current-voltage relationship.

3.4. The IF amino acid residues are important for current inactivation

To further assess the importance of the conserved IF residues of $Ca_V2.2$ in current inactivation, we co-expressed $Ca_V2.2^{IF/AF}$ or $Ca_V2.2^{IF/AA}$ with CaM and measured the currents (Fig. 4 and Table 1). Representative traces (Fig. 4A and B) of $Ca_V2.2^{IF/AF}$ and $Ca_V2.2^{IF/AA}$ showed a higher level of inactivation when using Ca^{2+} as the charge carrier than Ba^{2+}. Fig. 4C and D shows that the average R_{250}/Ca^{2+} of $Ca_V2.2^{IF/AF}$ and $Ca_V2.2^{IF/AA}$ was similar to that of $Ca_V2.2$; however, the R_{250}/Ba^{2+} was 68.5 ± 3.9% (n = 4, $p < 0.05$) and 57.7 ± 4.8% (n = 6, $p < 0.01$), respectively, which were both significantly lower than that of the wild-type form (79.0 ± 2.5%, n = 13). CaM_{12} significantly increased the R_{250}/Ca^{2+} of $Ca_V2.2^{IF/AF}$ to 45.2 ± 2.8% (n = 8, $p < 0.05$) compared to that of the CaM group, but CaM_{34} and CaM_{1234} had little effect on the R_{250}/Ca^{2+}. In contrast, the R_{250}/Ba^{2+} values for $Ca_V2.2^{IF/AF}$ with different CaM constructs were approximately the same in a range between 60 and 70%. For $Ca_V2.2^{IF/AA}$, the co-expression of CaM and mutants did not have any significant effect on the R_{250}/Ca^{2+} and R_{250}/Ba^{2+}. The activation curves of the wild-type and mutated channels co-expressing CaM and CaM mutants are shown in Fig. S1; the calculated $V_{1/2}$ and slope are listed in Table 1. These results suggest that mutations in the IF residues

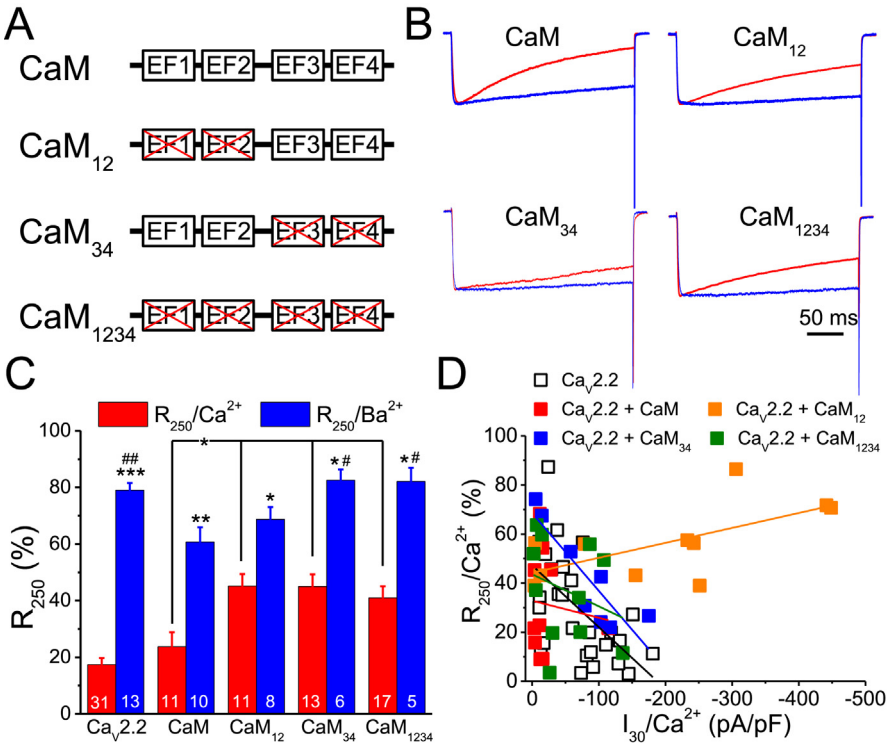

Fig. 2. Ca^{2+}-binding-deficient CaM mutants increase the R_{250}/Ca^{2+}. We co-expressed $Ca_V2.2$ with CaM and CaM mutants with binding deficiencies at the N-, C-, and both lobes (CaM_{12}, CaM_{34}, and CaM_{1234}, respectively) in HEK293T cells. The currents were recorded at +30 mV using Ca^{2+} or Ba^{2+} as the charge carrier, and the R_{250}/Ca^{2+} and R_{250}/Ba^{2+} were analyzed. A. Schematic representation of the CaM and CaM mutants. B. Representative normalized current traces (each trace was normalized to the inward peak current) from cells expressing CaM or mutants. C. Average R_{250}/Ca^{2+} and R_{250}/Ba^{2+}. The numbers on each column refer to the number of cells used in each group. Data are presented as the mean ± SEM and were analyzed by one-way ANOVA with Fisher's post hoc test. *: $p < 0.05$, **: $p < 0.01$, and ***: $p < 0.001$ compared to the same expression group using Ca^{2+} as the charge carrier. #: $p < 0.05$ and ##: $p < 0.001$ compared to the R_{250}/Ba^{2+} of the CaM group. D. Plot of R_{250}/Ca^{2+} against I_{30}/Ca^{2+}. The R_{250}/Ca^{2+} of each cell in Fig. 2C was plotted against the I_{30}/Ca^{2+}. The lines indicated the linear regression of each group.

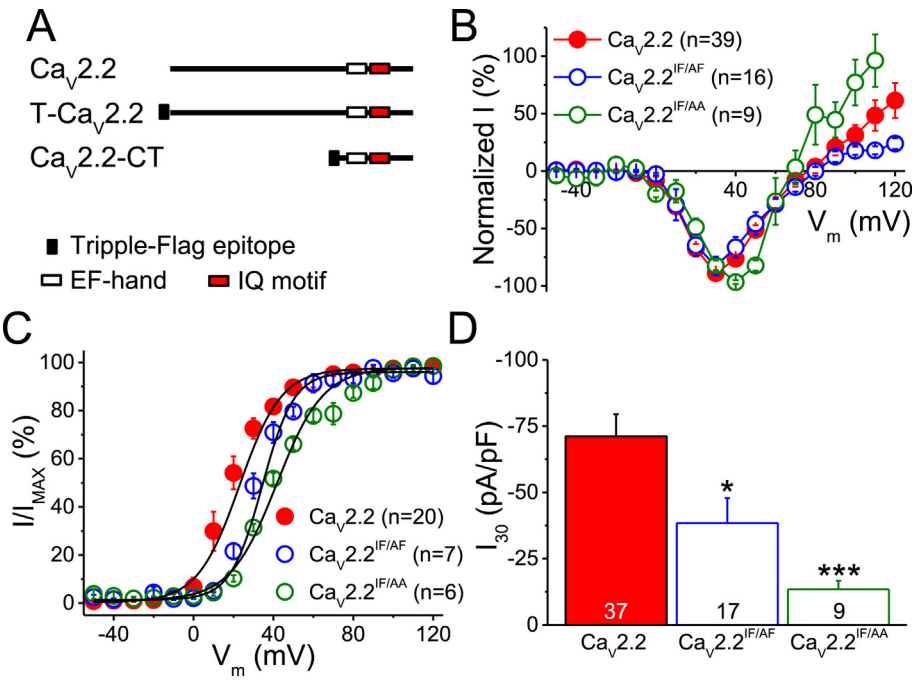

Fig. 3. Mutations in the IF residues of $Ca_V2.2$ reduce the current. $Ca_V2.2$ with mutations in the IF residues ($Ca_V2.2^{IF/AF}$ and $Ca_V2.2^{IF/AA}$) was expressed in the HEK293T cells. A. Schematic representation of $Ca_V2.2$ and the constructs. B. The current-voltage relationship. The cell was whole-cell patched and depolarized for 250 ms from a holding potential of −70 mV to various potentials using Ca^{2+} as the charge carrier. The peak current recorded at each potential was normalized to the inward maxima of each cell. C. The activation curves. Cells were depolarized for 10 ms from a holding potential of −70 mV to various potentials, and the tail inward current obtained at each potential was normalized to the maxima. D. The I_{30}/Ca^{2+} of $Ca_V2.2$ and the mutants. The current was evoked by a depolarization to +30 mV for 250 ms, and the peak inward current was measured. Data are presented as the mean ± SEM and were analyzed by one-way ANOVA with Fisher's post hoc test. *: $p < 0.05$ and ***: $p < 0.001$ compared to the wild-type.

blocked the effects of the CaM mutants, except CaM_{12}, in suppressing the current inactivation.

3.5. *CaM_{12} enhances the attenuated current density*

In addition to the effects on current inactivation, the mutations in the IF residues greatly reduced the current amplitude (Table 1). Compared to the group expressing $Ca_V2.2^{IF/AF}$ and CaM, which had an I_{30}/Ca^{2+} of −52.8 ± 15.0 pA/pF (n = 9), CaM_{12} substantially enhanced the I_{30}/Ca^{2+} to −109.5 ± 40.9 pA/pF (n = 7, $p < 0.05$); in contrast, CaM_{34} and CaM_{1234} slightly decreased the I_{30}/Ca^{2+} but not significantly. For $Ca_V2.2^{IF/AA}$, CaM, CaM_{12}, and CaM_{34} could slightly but not significantly enhance the I_{30}/Ca^{2+}. By plotting the R_{250}/Ca^{2+} against the I_{30}/Ca^{2+} (Fig. 2D) from cells expressing $Ca_V2.2$ and CaM/mutants, the linear regression curves showed an inverse relationship, except for the CaM_{12} group, which had a R_{250}/Ca^{2+} above 40% regardless of the current density. In addition, the I_{30}/Ba^{2+} were larger than those I_{30}/Ca^{2+} of the same groups except the CaM_{12} group (Table SI). For $Ca_V2.2$ wild type and mutants, the I_{30}/Ca^{2+} and I_{30}/Ba^{2+} were about the same in the co-expression of CaM_{12}. These results indicated that the conserved IF residues and each lobe of CaM are important in regulating the current density.

3.6. *Differential binding of CaM mutants to the C-terminal fragment of $Ca_V2.2$*

To confirm that CaM interacts with $Ca_V2.2$ at the C-terminal, we used GST-tagged CaM or Ca^{2+}-binding-deficient mutants as the bait to pull down $Ca_V2.2$-CT expressed in HEK293T cells (Fig. 5A–D). A representative Western blot shows that GST-CaM pulled down a protein with a MW similar to the expected size of $Ca_V2.2$-CT (~72 kD) in the presence of Ca^{2+} (100 μM), EGTA (5 μM), or no addition; however, GST-CaM_{12} and -CaM_{1234} could only interact with this fragment in the presence of Ca^{2+} but with a lower capacity than that of CaM. CaM_{34} did not show any interaction with the $Ca_V2.2$-CT. We then mutated the conserved IF residues to AA ($Ca_V2.2$-$CT^{IF/AA}$) for pulldown assays to characterize the importance of the IF residues in this interaction. Western blot analysis (Fig. 5E) showed that little $Ca_V2.2$-$CT^{IF/AA}$ was observed regardless of the presence of CaM or mutants with or without Ca^{2+}. These results illustrate the importance of the IF residues in the binding of CaM to $Ca_V2.2$ and indicate that each lobe of CaM has differential contributions to this interaction.

3.7. *CaM_{12} enhances the expression level of $Ca_V2.2$*

Because CaM and the mutants affected the I_{30}/Ca^{2+}, we examined the total expression level and the fraction of $Ca_V2.2$ localized at the cell membrane (Fig. 6). The lysates from cells transfected with $Ca_V2.2$ showed a protein band with a MW greater than 250 kD that was not observed in the control group without $Ca_V2.2$ expression (Fig. 6A). With co-expression of CaM and the mutants, the lysate containing CaM_{12} showed an increased band intensity compared to that of the other groups. The average total $Ca_V2.2$ level from cells co-expressing CaM_{12} was 1.6 ± 0.1 (n = 3, $p < 0.05$) when normalized to the group with CaM overexpression, which was significantly higher than that with CaM overexpression (Fig. 6B). CaM_{34} (1.1 ± 0.3) resulted in a similar level of $Ca_V2.2$ expression to that of the CaM group; CaM_{1234} (0.7 ± 0.3, n = 3, $p = 0.06$) slightly reduced the expression level but not significantly. Because the number of channels at the plasma membrane determines the current density, we used biotinylation to label the proteins at the plasma membrane and analyzed the ratio of $Ca_V2.2$ at the membrane to the total lysate (Fig. 6C–D). Western blot analysis showed that the antibody against $Ca_V2.2$ could recognize a protein in the biotinylation fraction with a MW similar to that in the total lysate. After analyzing the intensities of these bands, the $Ca_V2.2$ located at the membrane surface was 40–50% of the total $Ca_V2.2$ in all cell groups. These results indi-

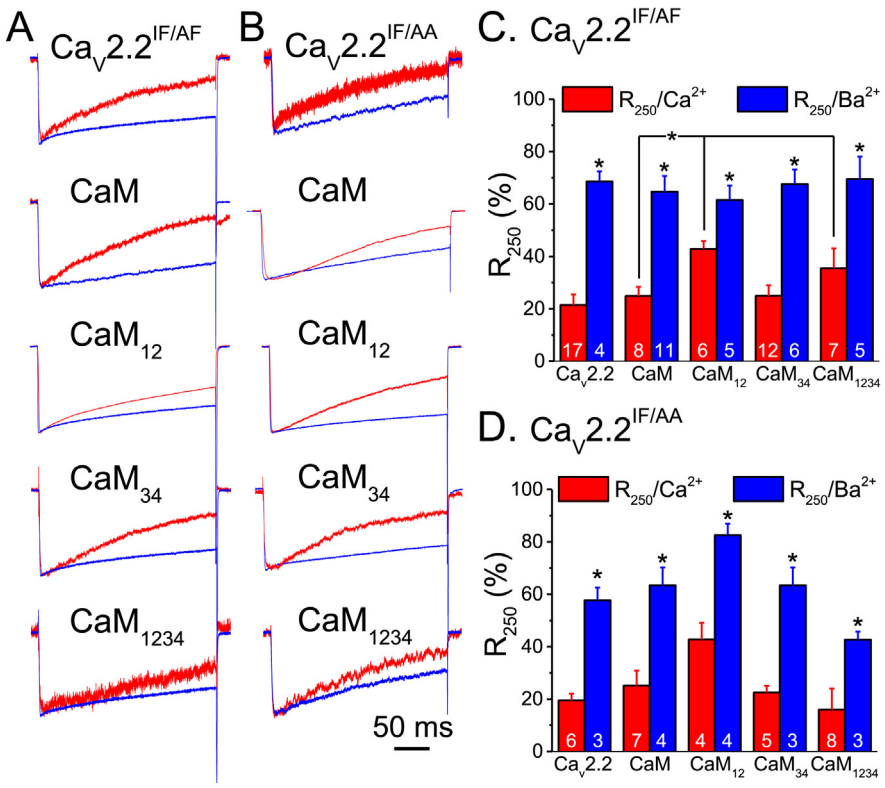

Fig. 4. CaM_{12} increases the R_{250}/Ca^{2+} of mutated $Ca_V2.2$. The conserved IF residues of $Ca_V2.2$ were mutated to AF ($Ca_V2.2^{IF/AF}$) or AA ($Ca_V2.2^{IF/AF}$) and expressed in HEK293T cells. A & B. The representative current traces from cells expressing $Ca_V2.2^{IF/AF}$ and $Ca_V2.2^{IF/AA}$ co-expressing CaM and CaM mutants. The patched cell was depolarized to +30 mV from a holding potential of −70 mV for 250 ms using Ca^{2+} (red traces) or Ba^{2+} (blue traces) as the charge carrier. C & D. Average R_{250} of $Ca_V2.2^{IF/AF}$ and $Ca_V2.2^{IF/AF}$, respectively. Data are presented as the mean ± SEM and were analyzed by one-way ANOVA with Fisher's post hoc test. *: $p < 0.05$ and ***: $p < 0.001$ compared to the same expression group or as indicated.

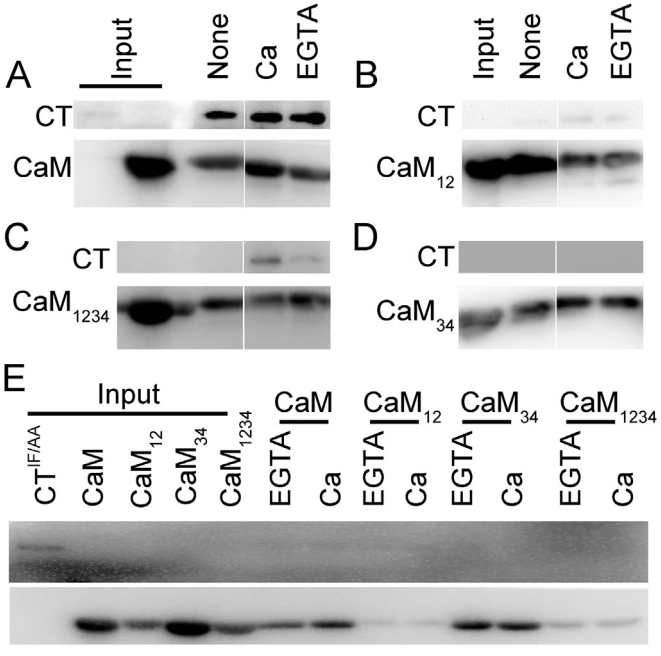

Fig. 5. CaM interacts with the C-tail fragment of $Ca_V2.2$. The lysates from HEK293T cells expressing the intracellular C-tail fragment of the wild-type (CT, 72 kDa) (A–D) or mutant $Ca_V2.2$ ($CT^{IF/AA}$) (E) were used for pulldown assays with GST-tagged CaM and mutants (43 kDa) as the baits. The reaction buffer for the assays had no extra addition (None) or contained 100 μM of Ca^{2+} (Ca) or 5 μM of EGTA (EGTA). The pull-down fraction was then analyzed by Western blotting using a monoclonal antibody against the C-terminal of $Ca_V2.2$ (CT) or CaM.

cate that CaM_{12} increases the total amount of $Ca_V2.2$ in the cells and plasma membrane.

4. Discussion

Ca^{2+} influx through the Ca_Vs is the major elicitor of exocytosis and many other Ca^{2+}-related activities in excitable cells; thus, regulating the kinetics of Ca_Vs could be an effective way to modulate different cellular functions (Dubel et al., 1992; Williams et al., 1992). Our results demonstrated that CaM binds to the conserved IQ motif of $Ca_V2.2$ at the intracellular C-terminal to trigger CDI. In addition, CaM_{12} enhanced the current amplitude and the total expression level of $Ca_V2.2$ at the cell membrane. Therefore, the N- and C-lobes of CaM have differential effects in regulating $Ca_V2.2$ activity.

For Ca_V1s, $Ca_V2.1$, and $Ca_V2.3$, binding of CaM to the C-terminal IQ motif determines the CDI (DeMaria et al., 2001; Yang et al., 2006). Several reports utilizing a gene-shuffled chimeric C-terminal of $Ca_V2.2$ and Ca_V1s have also suggested that CaM binds to the C-terminal end and promotes CDI of the chimeric channels (Kim et al., 2008; Mori et al., 2008). The IQ segments of $Ca_V2.1$-3 interact with CaM as determined by X-ray crystallography and isothermal titration calorimetry (Fallon et al., 2009; Kim et al., 2008; Wang et al., 2014). The X-ray structure analysis shows that the IQ-helix peptides of $Ca_V1.2$ and Ca_V2s bind the pocket of CaM in the opposite orientation. The N-lobe of CaM interacts more with the a. a. residues located at the N-terminal portion of the $Ca_V1.2$ IQ peptide relative to the conserved IQ residues but the C-terminal portion of the IQ peptide of the Ca_V2s and vice versa. Even so, the CDI is determined by the interaction between the CaM N-lobe and the C-terminal portion of the IQ motif; therefore, mutations at the N-lobe

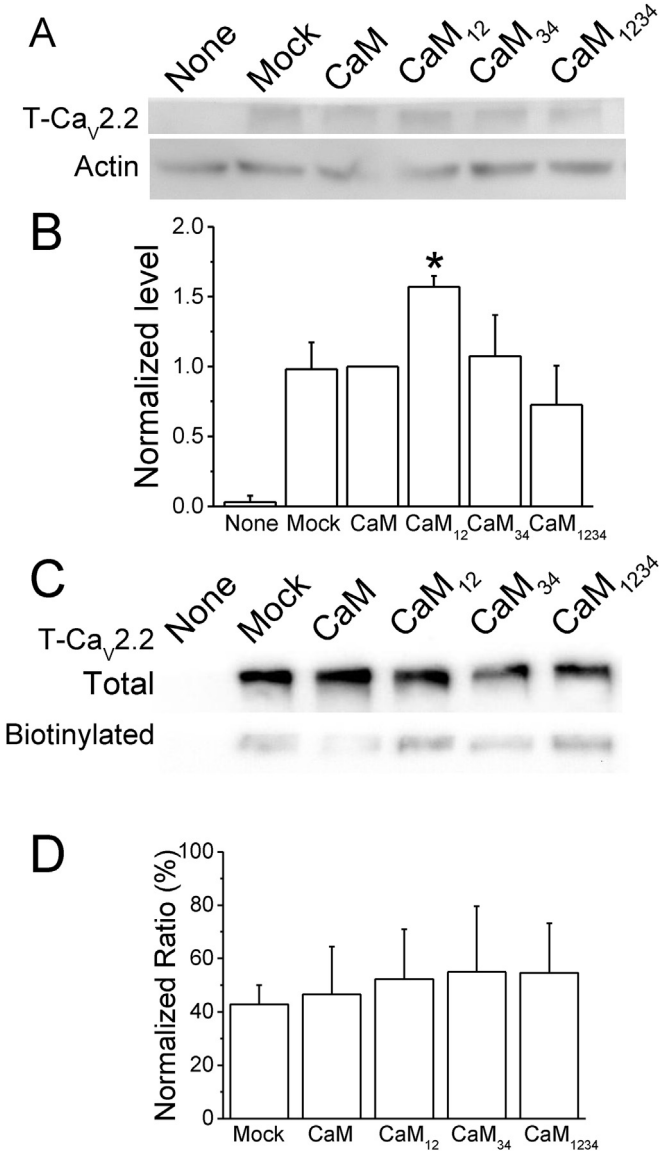

Fig. 6. CaM_{12} enhances the total expression level of $Ca_V2.2$. A. Representative Western blot of $Ca_V2.2$ in total lysates. Cell lysates isolated from HEK293T cells with no transfection (None), transfected with T-$Ca_V2.2$ only (T-$Ca_V2.2$, Mock), or transfected with co-expression of CaM, CaM_{12}, CaM_{34}, and CaM_{1234} were used for Western blot analysis using antibodies against FLAG and β-actin. B. Normalized total $Ca_V2.2$ level. The level of T-$Ca_V2.2$ was normalized to the level of β-actin in each sample; the values were then normalized to the value of the CaM group in each independent experiment. C. Representative staining of $Ca_V2.2$ after being biotinylated. Membrane proteins were first labeled with biotin and then isolated with avidin. The T-$Ca_V2.2$ in the total lysate (Total) and avidin-purified fraction (Biotinylated) was analyzed by an antibody against FLAG. D. The ratio of $Ca_V2.2$ in the membrane fraction to the total lysate. Data are presented as the mean ± SEM from at least 3 independent experiments and were analyzed by one-way ANOVA with Fisher's post hoc test. *: $p < 0.05$ compared to the CaM group.

(CaM_{12} and CaM_{1234}) lose the ability to induce CDI (Liang et al., 2003). However, our results showed that losing the Ca^{2+}-binding ability at either the N- or C-lobes of CaM decreases the CDI to a similar level, suggesting that either interaction is necessary and sufficient to maintain the CDI. We mutated the last a. a., E, in each EF-hand motif of CaM to Q to reduce the Ca^{2+}-binding capability, while Liang et al. (2003) converted the first residues, D, of each motif to A. This discrepancy may differentially affect the functions of CaM and explain the difference of the results.

An amino-terminal Ca^{2+}/CaM binding segment (NSCaTE, N-terminal Spatial Ca^{2+} Transforming Element) of $Ca_V1.3$ is known to interact with the N-lobe of CaM (Liu and Vogel, 2012). In the N-portion of the C-terminus of Ca_V1s and Ca_V2s, the pre-IQ domain and IQ domain are also CaM binding sites (Ben-Johny et al., 2015; Johny et al., 2013). The NSCaTE element can interact with Ca^{2+}/CaM prebound to an IQ domain peptide, suggesting the possible bridging of the channel amino- and carboxyl-termini; however, $Ca_V2.2$ does not contain the NSCaTE element (Taiakina et al., 2013). Therefore, CaM may interact with the $Ca_V2.2$ mostly through the intracellular C-terminal.

Here, using pulldown assays and current measurement, we further demonstrated that the binding of CaM to $Ca_V2.2$ is not Ca^{2+}-dependent, suggesting that CaM could interact with $Ca_V2.2$ at rest; in addition, the over-expression of CaM did not enhance the CDI, indicating that most $Ca_V2.2$ molecules are bound with CaM at rest, and a global elevation of $[Ca^{2+}]_i$ would activate the CDI (Ben-Johny and Yue, 2014; Dick et al., 2008, 2016; Few et al., 2012; Liang et al., 2003). The plot of the R_{250}/Ca^{2+} against the I_{30}/Ca^{2+} from cells expressing $Ca_V2.2$ shows an inverse relationship, supporting the global Ca^{2+} effect on current inactivation. The expression of CaM and the mutants showed an inverse relationship as well, except for CaM_{12}, which not only enhanced the I_{30}/Ca^{2+} but also maintained the R_{250}/Ca^{2+} above 40%. However, using Ba^{2+} as the charge carrier did not enhance the current amplitude in the co-expression of CaM_{12}. It is possible that CaM_{12} blocks the CDI even when the current density is high or increases the VDI portion of the evoked current. The mechanism by which CaM_{12} modulates the current inactivation needs to be investigated further.

In contrast to the wild-type CaM, the binding of CaM_{12} to $Ca_V2.2$-CT requires Ca^{2+}; therefore, when $[Ca^{2+}]_i$ is elevated, CaM_{12} competes with the endogenous bound CaM and increases the R_{250}/Ca^{2+}. Although CaM_{34} is incapable of binding to $Ca_V2.2$-CT, CaM_{34} may interfere with the interaction between endogenous CaM and $Ca_V2.2$ to increase the R_{250}/Ca^{2+}. The $Ca_V2.2$-CT we constructed includes a Ca^{2+}-binding motif (Delcour et al., 1993; Johny et al., 2013; Yang et al., 2006); upon Ca^{2+} binding, this motif may prepare $Ca_V2.2$-CT for CaM binding. As CaM can have different conformations when free or bound with Ca^{2+} (Fallon et al., 2009; Hultschig et al., 2004), CaM with a mutated N-lobe (CaM_{12} and CaM_{1234}) may have a conformation that allows Ca^{2+}-dependent binding to $Ca_V2.2$.

The binding of CaM to the IQ motif of $Ca_V2.2$ is important in maintaining the current amplitude as mutations in the conserved IF residues greatly reduced the I_{30}/Ca^{2+}, and the overexpression of CaM, especially CaM_{12}, rescued the current amplitude of these mutants. The pulldown assays showed that CaM and the mutants did not bind to $Ca_V2.2$-$CT^{IF/AA}$, and CaM_{12} overexpression increased the total amount of $Ca_V2.2$ expressed in HEK293T cells but did not affect the fraction of $Ca_V2.2$ at the plasma membrane (Fig. 6). This may partly explain how CaM_{12} overexpression enhances the current. However, it is not clear how CaM_{12} modulates the R_{250}/Ca^{2+} level. It is possible that most of the current either enhanced by CaM_{12} or decreased by the channel mutations was due to CDI, but this needs to be further characterized.

The β and $\alpha_2\delta$ subunits of Ca_Vs are involved in modulating the kinetics and amplitude of the currents, as well as targeting the channels to the plasma membrane (Brice and Durward, 1997; Singer et al., 1991). The transient over-expression of $\alpha_2\delta$-1, $\alpha_2\delta$-2 and $\alpha_2\delta$-3 subunits in cultured hippocampal neurons increases not only the presynaptic abundance of P/Q-type channels but the probability of vesicular release in response to a single action potential (Hoppa et al., 2012). The cytosolic β subunits have a chaperone-like effect in promoting the functional expression of the subunits of Ca_V2s at the plasma membrane (Bichet et al., 2000; Brice and Durward, 1997; Raghib et al., 2001). In addition, β subunits control the gating properties of the Ca_Vs and hyperpolarize the voltage-dependence of activation, as well as increase the maximum open

Table 1
The basic properties of $Ca_V2.2$ with mutations in the IQ motif.

Co-expression		$V_{1/2}$ (mV)	Slope (mV)	I_{30}/Ca^{2+} (pA/pF)	R_{250}/Ca^{2+} (%)	R_{250}/Ba^{2+} (%)
$Ca_V2.2$	Mock	18.7 ± 2.7	6.2 ± 0.8	−71.1 ± 8.4	17.4 ± 2.3	79.0 ± 2.5
		n = 20	n = 20	n = 37	n = 31	n = 13
	CaM	13.5 ± 2.7	4.6 ± 1.0	−29.9 ± 11.7*	23.8 ± 5.1	60.7 ± 5.2*
		n = 8	n = 8	n = 10	n = 11	n = 10
	CaM_{12}	24.7 ± 2.4	7.1 ± 0.6	−170.3 ± 25.7**	45.1 ± 4.2*	68.7 ± 4.3*
		n = 4	n = 4	n = 6	n = 11	n = 8
	CaM_{34}	25.5 ± 3.2	7.7 ± 1.3	−78.0 ± 16.5	45.0 ± 4.3*	82.5 ± 3.8
		n = 5	n = 5	n = 8	n = 13	n = 6
	CaM_{1234}	21.9 ± 2.9	5.9 ± 0.8	−51.8 ± 11.3*	41.0 ± 4.1*	82.1 ± 4.8
		n = 16	n = 16	n = 11	n = 17	n = 5
$Ca_V2.2^{IF/AF}$	Mock	31.6 ± 1.9	8.8 ± 1.2	−38.5 ± 9.4	21.5 ± 4.0	68.5 ± 3.9
		n = 7	n = 7	n = 17	n = 17	n = 4
	CaM	26.2 ± 3.4	8.6 ± 1.9	−52.8 ± 15.0	24.9 ± 3.5	64.7 ± 6.0
		n = 5	n = 5	n = 9	n = 8	n = 11
	CaM_{12}	15.4 ± 5.7	6.8 ± 1.6	−109.5 ± 40.9	45.2 ± 2.8	61.5 ± 5.5
		n = 5	n = 5	n = 7	n = 8	n = 5
	CaM_{34}	37.7 ± 2.5	14.2 ± 3.2	−23.7 ± 7.9	25.0 ± 4.1	67.6 ± 5.5
		n = 5	n = 5	n = 12	n = 12	n = 6
	CaM_{1234}	30.7 ± 2.8	9.1 ± 0.6	−33.3 ± 9.3	33.5 ± 7.6	69.5 ± 8.6
		n = 5	n = 5	n = 16	n = 7	n = 5
$Ca_V2.2^{IF/AA}$	Mock	41.4 ± 2.0	13.2 ± 1.1	−13.4 ± 3.3	19.5 ± 2.6	57.7 ± 4.8
		n = 6	n = 6	n = 9	n = 6	n = 6
	CaM	30.0 ± 4.9	7.9 ± 2.1	−60.5 ± 19.9	25.2 ± 5.7	63.4 ± 6.8
		n = 6	n = 6	n = 9	n = 7	n = 4
	CaM_{12}	10.6 ± 13.1	6.4 ± 2.1	−118.8 ± 41.3	37.8 ± 5.6	82.6 ± 4.3
		n = 3	n = 3	n = 4	n = 6	n = 4
	CaM_{34}	7.6 ± 10.1	0.8 ± 0.5	−63.1 ± 20.3	22.5 ± 2.6	63.4 ± 6.8
		n = 3	n = 3	n = 7	n = 5	n = 3
	CaM_{1234}	25.0 ± 6.4	8.1 ± 2.5	−20.0 ± 4.4	16.0 ± 8.1	42.7 ± 3.1
		n = 4	n = 4	n = 9	n = 8	n = 3

Data are presented as the mean ± SEM and were analyzed by one-way ANOVA with Fisher's post hoc test. *: $p < 0.05$ and **: $p < 0.01$ when compared to the Mock group.

probability resulting in increasing the macroscopic current density (Matsuyama et al., 1999; Meir et al., 2000; Neely et al., 1993). Our results showed that CaM_{12} could enhance the total expression level of $Ca_V2.2$ but not the ratio of the membrane localization. It is not clear how CaM regulates the membrane targeting of $Ca_V2.2$ and needs to be further characterized.

5. Conclusion

Our findings suggest that CaM binds to $Ca_V2.2$ via the conserved IQ motif to modulate the expression level and current density at rest or low $[Ca^{2+}]_i$; when $[Ca^{2+}]_i$ elevates, the bound CaM enhances CDI. Because CaM_{12} and CaM_{34} show different effects in modulating these above-mentioned activities, the N- and C-lobes of CaM work differentially in modulating $Ca_V2.2$. In addition to providing various binding sites for activity regulation, the C-terminus of $Ca_V1.2$ and $Ca_V2.1$ could be cleaved by a protease, such as calpain, and the dissociated distal fragments may either interact with the proximal C-terminus to inhibit the channel activity or translocate to the nucleus, acting as a transcription factor (Abele and Yang, 2012; Hell et al., 1996). These results reveal that the versatile pathways for regulating channel activity via the C-terminus of Ca_Vs and CaM, with different Ca^{2+}-binding abilities, are an immediate regulatory factor for various cellular functions (Ben-Johny et al., 2015).

Acknowledgments and conflict of interest disclosure

This work was supported by the Ministry of Science and Technology of Taiwan under grant Nos. of MOST 104-2627-M-002-003 and 103-2320-B-002-060-MY3. Technical support from *Technology Commons*, *College of Life Science*, *National Taiwan University (Taiwan)* is also acknowledged.

Appendix A. Supplementary data

Supplementary data related to this article can be found at http://dx.doi.org/10.1016/j.ibror.2017.03.002.

References

Abele, K., Yang, J., 2012. Regulation of voltage-gated calcium channels by proteolysis. Sheng Li Xue Bao 64, 504–514.
Ben-Johny, M., Dick, I.E., Sang, L., Limpitikul, W.B., Kang, P.W., Niu, J., Banerjee, R., Yang, W., Babich, J.S., Issa, J.B., et al., 2015. Towards a unified theory of calmodulin regulation (calmodulation) of voltage-gated calcium and sodium channels. Curr. Mol. Pharmacol. 8, 188–205.
Ben-Johny, M., Yue, D.T., 2014. Calmodulin regulation (calmodulation) of voltage-gated calcium channels. J. Gen. Physiol. 143, 679–692.
Berridge, M.J., 2014. Calcium signalling and psychiatric disease: bipolar disorder and schizophrenia. Cell Tissue Res. 357, 477–492.
Bichet, P., Mollat, P., Capdevila, C., Sarubbi, E., 2000. Endogenous glutathione-binding proteins of insect cell lines: characterization and removal from glutathione S-transferase (GST) fusion proteins. Protein Expr. Purif. 19, 197–201.
Brice, E., Durward, H., 1997. Multidisciplinary records: a step in the right direction? Paediatr. Nurs. 9, 26–27.
Chaudhuri, D., Issa, J.B., Yue, D.T., 2007. Elementary mechanisms producing facilitation of $Ca_V2.1$ (P/Q-type) channels. J. Gen. Physiol. 129, 385–401.
Chou, A.C., Ju, Y.T., Pan, C.Y., 2015. Calmodulin interacts with the sodium/calcium exchanger NCX1 to regulate activity. PLoS One 10, e0138856.
Coppola, T., Waldmann, R., Borsotto, M., Heurteaux, C., Romey, G., Mattei, M.G., Lazdunski, M., 1994. Molecular cloning of a murine N-type calcium channel alpha 1 subunit. Evidence for isoforms, brain distribution, and chromosomal localization. FEBS Lett. 338, 1–5.
Currie, K.P., Fox, A.P., 2002. Differential facilitation of N- and P/Q-type calcium channels during trains of action potential-like waveforms. J. Physiol. 539, 419–431.
Delcour, A.H., Lipscombe, D., Tsien, R.W., 1993. Multiple modes of N-type calcium channel activity distinguished by differences in gating kinetics. J. Neurosci. 13, 181–194.
DeMaria, C.D., Soong, T.W., Alseikhan, B.A., Alvania, R.S., Yue, D.T., 2001. Calmodulin bifurcates the local Ca^{2+} signal that modulates P/Q-type Ca^{2+} channels. Nature 411, 484–489.
Dick, I.E., Limpitikul, W.B., Niu, J., Banerjee, R., Issa, J.B., Ben-Johny, M., Adams, P.J., Kang, P.W., Lee, S.R., Sang, L., et al., 2016. A rendezvous with the queen of ion channels: three decades of ion channel research by David T Yue and his calcium signals laboratory. Channels (Austin) 10, 20–32.

Dick, I.E., Tadross, M.R., Liang, H., Tay, L.H., Yang, W., Yue, D.T., 2008. A modular switch for spatial Ca^{2+} selectivity in the calmodulin regulation of Ca_V channels. Nature 451, 830–834.
Dubel, S.J., Starr, T.V., Hell, J., Ahlijanian, M.K., Enyeart, J.J., Catterall, W.A., Snutch, T.P., 1992. Molecular cloning of the alpha-1 subunit of an omega-conotoxin-sensitive calcium channel. Proc. Natl. Acad. Sci. U. S. A. 89, 5058–5062.
Dunlap, K., Luebke, J.I., Turner, T.J., 1995. Exocytotic Ca^{2+} channels in mammalian central neurons. Trends Neurosci. 18, 89–98.
Eckert, R., Chad, J.E., 1984. Inactivation of Ca^{2+} channels. Prog. Biophys. Mol. Biol. 44, 215–267.
Eckert, R., Tillotson, D.L., 1981. Calcium-mediated inactivation of the calcium conductance in caesium-loaded giant neurones of Aplysia californica. J. Physiol. 314, 265–280.
Fallon, J.L., Baker, M.R., Xiong, L., Loy, R.E., Yang, G., Dirksen, R.T., Hamilton, S.L., Quiocho, F.A., 2009. Crystal structure of dimeric cardiac L-type calcium channel regulatory domains bridged by Ca2+* calmodulins. Proc. Natl. Acad. Sci. U. S. A. 106, 5135–5140.
Few, A.P., Nanou, E., Watari, H., Sullivan, J.M., Scheuer, T., Catterall, W.A., 2012. Asynchronous Ca^{2+} current conducted by voltage-gated $Ca_V2.1$ and $Ca_V2.2$ channels and its implications for asynchronous neurotransmitter release. Proc. Natl. Acad. Sci. U. S. A. 109, E452–E460.
Fujita, Y., Mynlieff, M., Dirksen, R.T., Kim, M.S., Niidome, T., Nakai, J., Friedrich, T., Iwabe, N., Miyata, T., Furuichi, T., et al., 1993. Primary structure and functional expression of the omega-conotoxin-sensitive N-type calcium channel from rabbit brain. Neuron 10, 585–598.
Hell, J.W., Westenbroek, R.E., Breeze, L.J., Wang, K.K., Chavkin, C., Catterall, W.A., 1996. N-methyl-D-aspartate receptor-induced proteolytic conversion of postsynaptic class C L-type calcium channels in hippocampal neurons. Proc. Natl. Acad. Sci. U. S. A. 93, 3362–3367.
Hoppa, M.B., Lana, B., Margas, W., Dolphin, A.C., Ryan, T.A., 2012. alpha2delta expression sets presynaptic calcium channel abundance and release probability. Nature 486, 122–125.
Hultschig, C., Hecht, H.J., Frank, R., 2004. Systematic delineation of a calmodulin peptide interaction. J. Mol. Biol. 343, 559–568.
Johny, M.B., Yang, P.S., Bazzazi, H., Yue, D.T., 2013. Dynamic switching of calmodulin interactions underlies Ca^{2+} regulation of $Ca_V1.3$ channels. Nat. Commun. 4, 1717.
Kim, E.Y., Rumpf, C.H., Fujiwara, Y., Cooley, E.S., Van Petegem, F., Minor Jr., D.L., 2008. Structures of Ca_V2 Ca^{2+}/CaM-IQ domain complexes reveal binding modes that underlie calcium-dependent inactivation and facilitation. Structure 16, 1455–1467.
Lee, A., Scheuer, T., Catterall, W.A., 2000. Ca^{2+}/calmodulin-dependent facilitation and inactivation of P/Q-type Ca^{2+} channels. J. Neurosci. 20, 6830–6838.
Lian, H., Zheng, H., 2016. Signaling pathways regulating neuron-glia interaction and their implications in Alzheimer's disease. J. Neurochem. 136, 475–491.
Liang, H., DeMaria, C.D., Erickson, M.G., Mori, M.X., Alseikhan, B.A., Yue, D.T., 2003. Unified mechanisms of Ca^{2+} regulation across the Ca^{2+} channel family. Neuron 39, 951–960.
Lin, T.Y., Li, B.R., Tsai, S.T., Chen, C.W., Chen, C.H., Chen, Y.T., Pan, C.Y., 2013. Improved silicon nanowire field-effect transistors for fast protein-protein interaction screening. Lab. Chip 13, 676–684.
Liu, Z., Vogel, H.J., 2012. Structural basis for the regulation of L-type voltage-gated calcium channels: interactions between the N-terminal cytoplasmic domain and Ca^{2+}-calmodulin. Front. Mol. Neurosci. 5, 38.
Matsuyama, Z., Wakamori, M., Mori, Y., Kawakami, H., Nakamura, S., Imoto, K., 1999. Direct alteration of the P/Q-type Ca^{2+} channel property by polyglutamine expansion in spinocerebellar ataxia 6. J. Neurosci. 19, RC14.
Meir, A., Bell, D.C., Stephens, G.J., Page, K.M., Dolphin, A.C., 2000. Calcium channel beta subunit promotes voltage-dependent modulation of $\alpha 1B$ by $G_{\beta\gamma}$. Biophys. J. 79, 731–746.
Mills, L.R., Niesen, C.E., So, A.P., Carlen, P.L., Spigelman, I., Jones, O.T., 1994. N-type Ca^{2+} channels are located on somata, dendrites, and a subpopulation of dendritic spines on live hippocampal pyramidal neurons. J. Neurosci. 14, 6815–6824.
Mintz, I.M., Sabatini, B.L., Regehr, W.G., 1995. Calcium control of transmitter release at a cerebellar synapse. Neuron 15, 675–688.
Mori, M.X., Vander Kooi, C.W., Leahy, D.J., Yue, D.T., 2008. Crystal structure of the Ca_V2 IQ domain in complex with Ca^{2+}/calmodulin: high-resolution mechanistic implications for channel regulation by Ca^{2+}. Structure 16, 607–620.
Neely, A., Wei, X., Olcese, R., Birnbaumer, L., Stefani, E., 1993. Potentiation by the beta subunit of the ratio of the ionic current to the charge movement in the cardiac calcium channel. Science 262, 575–578.
Olivera, B.M., Miljanich, G.P., Ramachandran, J., Adams, M.E., 1994. Calcium channel diversity and neurotransmitter release: the omega-conotoxins and omega-agatoxins. Annu. Rev. Biochem. 63, 823–867.
Peterson, B.Z., DeMaria, C.D., Adelman, J.P., Yue, D.T., 1999. Calmodulin is the Ca^{2+} sensor for Ca^{2+} -dependent inactivation of L-type calcium channels. Neuron 22, 549–558.
Raghib, A., Bertaso, F., Davies, A., Page, K.M., Meir, A., Bogdanov, Y., Dolphin, A.C., 2001. Dominant-negative synthesis suppression of voltage-gated calcium channel Cav2.2 induced by truncated constructs. J. Neurosci. 21, 8495–8504.
Shih, P.Y., Lin, C.L., Cheng, P.W., Liao, J.H., Pan, C.Y., 2009. Calneuron I inhibits Ca^{2+} channel activity in bovine chromaffin cells. Biochem. Biophys. Res. Commun. 388, 549–553.
Simms, B.A., Zamponi, G.W., 2014. Neuronal voltage-gated calcium channels: structure, function, and dysfunction. Neuron 82, 24–45.
Simons, T.J., 1988. Calcium and neuronal function. Neurosurg. Rev. 11, 119–129.
Singer, D., Biel, M., Lotan, I., Flockerzi, V., Hofmann, F., Dascal, N., 1991. The roles of the subunits in the function of the calcium channel. Science 253, 1553–1557.
Soderling, T.R., Derkach, V.A., 2000. Postsynaptic protein phosphorylation and LTP. Trends Neurosci. 23, 75–80.
Soong, T.W., DeMaria, C.D., Alvania, R.S., Zweifel, L.S., Liang, M.C., Mittman, S., Agnew, W.S., Yue, D.T., 2002. Systematic identification of splice variants in human P/Q-type channel alpha1(2.1) subunits: implications for current density and Ca^{2+}-dependent inactivation. J. Neurosci. 22, 10142–10152.
Tadross, M.R., Dick, I.E., Yue, D.T., 2008. Mechanism of local and global Ca^{2+} sensing by calmodulin in complex with a Ca^{2+} channel. Cell 133, 1228–1240.
Taiakina, V., Boone, A.N., Fux, J., Senatore, A., Weber-Adrian, D., Guillemette, J.G., Spafford, J.D., 2013. The calmodulin-binding, short linear motif, NSCaTE is conserved in L-type channel ancestors of vertebrate $Ca_V1.2$ and $Ca_V1.3$ channels. PLoS One 8, e61765.
Tillotson, D., 1979. Inactivation of Ca conductance dependent on entry of Ca ions in molluscan neurons. Proc. Natl. Acad. Sci. U. S. A. 76, 1497–1500.
Wang, C., Chung, B.C., Yan, H., Wang, H.G., Lee, S.Y., Pitt, G.S., 2014. Structural analyses of Ca^{2+}/CaM interaction with Na_V channel C-termini reveal mechanisms of calcium-dependent regulation. Nat. Commun. 5, 4896.
Westenbroek, R.E., Hell, J.W., Warner, C., Dubel, S.J., Snutch, T.P., Catterall, W.A., 1992. Biochemical properties and subcellular distribution of an N-type calcium channel alpha 1 subunit. Neuron 9, 1099–1115.
Westenbroek, R.E., Hoskins, L., Catterall, W.A., 1998. Localization of Ca^{2+} channel subtypes on rat spinal motor neurons, interneurons, and nerve terminals. J. Neurosci. 18, 6319–6330.
Williams, M.E., Brust, P.F., Feldman, D.H., Patthi, S., Simerson, S., Maroufi, A., McCue, A.F., Velicelebi, G., Ellis, S.B., Harpold, M.M., 1992. Structure and functional expression of an omega-conotoxin-sensitive human N-type calcium channel. Science 257, 389–395.
Yagami, T., Kohma, H., Yamamoto, Y., 2012. L-type voltage-dependent calcium channels as therapeutic targets for neurodegenerative diseases. Curr. Med. Chem. 19, 4816–4827.
Yang, P.S., Alseikhan, B.A., Hiel, H., Grant, L., Mori, M.X., Yang, W., Fuchs, P.A., Yue, D.T., 2006. Switching of Ca^{2+}-dependent inactivation of $Ca_V1.3$ channels by calcium binding proteins of auditory hair cells. J. Neurosci. 26, 10677–10689.
Zweifach, A., Lewis, R.S., 1995. Slow calcium-dependent inactivation of depletion-activated calcium current. Store-dependent and -independent mechanisms. J. Biol. Chem. 270, 14445–14451.